A Broadband Multipole Method for Accelerated Mutual Coupling Analysis of Large Irregular Arrays Including Rotated Antennas

Quentin Gueuning, Eloy de Lera Acedo, Anthony Keith Brown, *Life Senior Member, IEEE*, Christophe Craeye, *Senior Member, IEEE*, and Oscar O'Hara

***Abstract*— We present a numerical method for the analysis of mutual coupling (MC) effects in large, dense, and irregular arrays with identical antennas. Building on the method-of-moments (MoM), our technique uses a macro-basis function (MBF) approach for rapid direct inversion of the MoM impedance matrix. To expedite the reduced matrix filling, we propose an extension of the steepest-descent multipole (SDM) expansion which remains numerically stable and efficient across a wide bandwidth. This broadband multipole-based approach is well-suited to quasi-planar problems and requires only the precomputation of each MBF's complex patterns, resulting in low antenna-dependent preprocessing costs. The method also supports arrays with arbitrarily rotated antennas at low additional cost. A simulation of all embedded element patterns (EEPs) of irregular arrays of 256 complex log-periodic antennas completes in just 10 min per frequency point on a current laptop, with an additional minute per new layout.**

***Index Terms*— Antenna arrays, broadband, macro-basis functions (MBFs), multipole method, mutual coupling (MC), quasi-planar, square kilometer array, steepest-descent path (SDP), wideband.**

I. Introduction

Mutual coupling (MC) refers to the electromagnetic interaction between antennas in an array, causing each element to behave differently, depending on its environment. The MC effect manifests itself as angular and frequency variations in the radiated far-fields, known as embedded element patterns (EEPs), among elements in the array and in the array impedance matrix. When not carefully accounted for by design, MC can cause nulls in radiation patterns [1] or impedance mismatches [2] between antennas and first-stage amplifiers. For instance, positioning antennas irregularly [4] or sequentially rotating them [5], [6], [7] can help randomize MC effects. This mutual interaction can be significant in wideband arrays due to the inherent antennas' support for higher order current modes. Given the widespread use of large wideband phased array systems [8] in radar, space communication, biomedical imaging, radio astronomy, and mobile communications, accurate modeling of each element's response in the presence of MC is important and enables the mitigation of undesired effects through the optimization of antenna geometry, array layout, and the integration with front-end electronics.

Analyzing MC requires solving Maxwell's equations using full-wave solvers capable of handling large, multiscale problems. Wideband antennas often have intricate geometries needing hundreds [9] or thousands [10] of mesh elements, while array sizes can extend to hundreds of wavelengths [11]. In addition, fine frequency resolution is required to capture severely narrowband MC effects [12]. General-purpose solvers based on the method-of-moments (MoM, [13]) often result in prohibitive computation times; that is, days or weeks per frequency on large workstations, even when accelerated with the multilevel fast multipole method (MLFMM, [14]) [15]). The irregularity of the layout also prevents the use of periodic boundary conditions. In contrast, fast computational electromagnetics (CEM) methods have been developed specifically for large irregular arrays, reducing potentially computation times to minutes/hours on a laptop [9], [16], [17], [18].

Solving the MoM system of equations for dense and electrically large problems is costly due to filling and inverting the impedance matrix, therefore requiring acceleration techniques. For array problems with identical and disconnected antennas, direct inversion techniques [9], [17], [19], [20], [21], [22], [23], [24], [25] are preferred over iterative ones [18], [26], [27] to avoid the use of preconditioners and to allow quick solutions for each excited array port. Frameworks such as macro-basis function (MBF, [22]), characteristic-basis function (CBF, [23]) or synthetic function expansion (SFX, [24]) enable direct matrix inversion by defining current basis functions over the antenna domain, hence reducing the number of unknowns per antenna. Despite reducing inversion costs, the impedance filling time remains equivalent to that of the brute-force (BF) MoM and must thus also be sped up. This can be achieved by modeling MBF interactions as a function of baselines using interpolative methods or analytical field expansions in a

Received 24 July 2024; revised 8 December 2024; accepted 1 January 2025. Date of publication 17 January 2025; date of current version 7 May 2025. This work was supported by the Science and Technology Facilities Council (STFC). The work of Quentin Gueuning was supported under Grant ST/W00206X/1. The work of Eloy de Lera Acedo was supported by STFC through Ernest Rutherford Fellowship (ERF) under Grant ST/V004425/1. The work of Oscar O'Hara was supported by the Design of Highly Sensitive EM Sensors for Space Applications under Grant G109464. *(Corresponding author: Quentin Gueuning.)*

Quentin Gueuning, Eloy de Lera Acedo, and Oscar O'Hara are with the Astrophysics Group, Cavendish Laboratory, and the Kavli Institute for Cosmology, Cavendish Laboratory, University of Cambridge, CB3 0HE Cambridge, U.K. (e-mail: quentin.gueuning@hotmail.com).

Anthony Keith Brown is with the School of Electrical and Electronic Engineering, Queen Mary University of London, E1 4NS London, U.K., and also with the Department of Electrical and Electronic Engineering, The University of Manchester, M13 9PL Manchester, U.K.

Christophe Craeye is with the Institute of Information and Communication Technologies, Electronics and Applied Mathematics (ICTEAM), Université Catholique de Leuven, 1348 Leuven-la-Neuve, Belgium.

Digital Object Identifier 10.1109/TAP.2025.3528766

precomputation step that is independent of array configuration. One approach, devised in [20], uses Rokhlin's multipole expansion [14], but it suffers from a low-frequency (LF) breakdown [28], limiting its use for interelement distances greater than about half a wavelength. Alternative schemes, such as those [9], [18] based on adaptive cross-approximation (ACA, [29]) and the harmonic-polynomial method (HARP, [17], [19]), build MBF interaction models from a few (entries of) precomputed elementary MoM blocks. For complex antennas meshed with many elements, these precomputations can take hours to days hindering fast frequency sweeping or recomputation for various antenna geometries. In contrast, the multipole-based approach [20] only requires precomputation of each MBFs' far-field patterns but cannot be used at short distances. This article thus proposes an alternative efficient multipole expansion for quasi-planar structures that remains free from LF breakdown.

The fast multipole method (FMM, [14]) is highly efficient in CEM, accelerating computations by factorizing MoM interactions between a source and an observation group into a sum of plane-wave interactions involving the product of source and observation patterns with an analytical translation function, which depends only on the vector relative distance between groups. While effective for large relative distances, the multipole expansion loses accuracy when groups are closer than about half a wavelength due to the LF breakdown [30]. Intense efforts [31], [32], [33], [34], [35], [36], [37], [38] have focused on deriving a broadband multipole expansion for general 3-D problems that remains accurate and efficient from low to high frequencies. One class of methods relies on a combination of LF-stable multipole [31], [32], [34] or algebraic methods such as QR decomposition [35] at lower frequencies, then transitioning to the MLFMM at higher frequencies. Another popular approach involves spectral-domain techniques [36], [37], [38], which are typically formulated by evaluating the Weyl identity [39] along a specific contour in the complex plane to include the evanescent part of the spectrum at low frequencies, thereby better capturing reactive near fields. However, this spectral decomposition is only numerically accurate in limited spatial sectors, thus requiring a partitioning of the observation domain with different sets of complex patterns for each sector. To the author's best knowledge, no single broadband multipole-based expansion has been derived for general 3-D problems yet. Interestingly, such expansions have been derived [28], [40], [41] for 2-D problems, effectively mitigating the LF breakdown with a simple renormalization procedure.

In this article, we propose a broadband multipole-based decomposition that extends the approach in [40] to address quasi-planar problems with small height over horizontal size ratio, as illustrated in Fig. 1. This is achieved by substituting the 2-D multipole expansion into a line-source expansion of the 3-D GF, akin to the high-frequency steepest-descent fast multipole method (SDFMM, [26]). The steepest-descent multipole (SDM) expansion thus includes the 2-D multipole translation function and numerical integration along the wavenumber k_z, perpendicular to the array's horizontal plane along the steepest-descent path (SDP). At high frequencies,

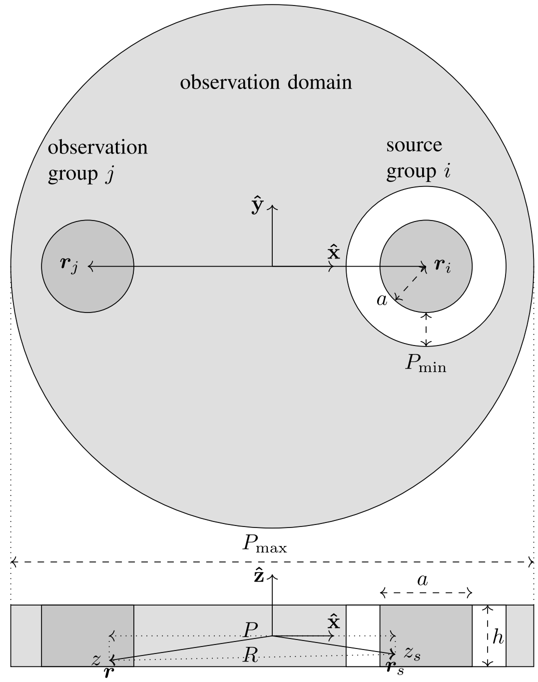

Fig. 1. Illustration of the quasi-planar geometry, characterized by a small height-to-diameter ratio. The figure shows in-plane (top) and vertical (bottom) cross sections, highlighting key parameters: height h, in-plane maximum and minimum distances $P_{\max}$ and $P_{\min}$, and the source and observation group radii a.

the SDM approach is more efficient for quasi-planar structures than standard 3-D multipole expansions [14], as it requires only plane waves propagating near the horizontal plane rather than across the entire sphere. At low frequencies, when antennas in dense wideband arrays are very close to each other, the required number of evanescent waves is drastically reduced using a nonuniform sampling scheme along k_z, as devised in [25] and [42]. Since this broadband multipole method requires only precomputation of complex patterns, i.e., far-field radiation patterns evaluated continuously both inside and outside the visible domain, for each MBF, the preprocessing step is cost-effective. This facilitates more efficient frequency sweeping and recomputation for various antenna geometries. In addition, our method allows for the arbitrary rotation of antennas at low additional computational cost. We demonstrate that full simulations with arrays of 256 wideband log-periodic antennas can be completed in just 10 min on a laptop, providing a significant performance improvement compared with FEKO's MLFMM [43], which is also constrained by the LF breakdown, and to HARP [17].

This article is organized as follows. Section II recalls the SDM expansion of the free-space GF. In Section III, we then identify the two numerical issues appearing at subwavelength distances. The broadband expansion resolving these issues is presented in Section IV. This expansion is then used to accelerate the MoM solver described in Section V. Numerical examples are presented in Section VI. Finally, conclusions are drawn in Section VII.

II. Reminder on the SDM Expansion of the 3-D Free-Space GF

In this article, we consider a quasi-planar structure confined within a cylinder of height h and diameter $P_{\max}$, as shown

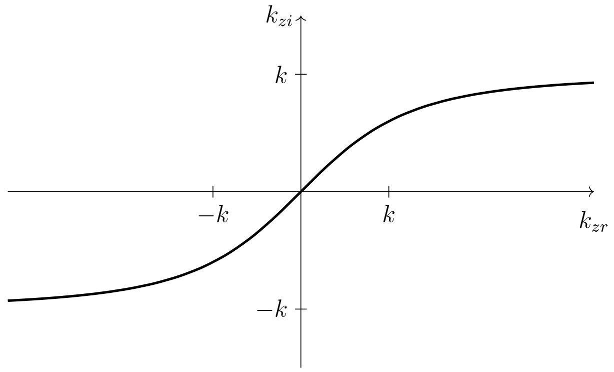

Fig. 2. Visualization of the SDP in the complex plane for integrating the 3-D GF. The SDP avoids the real-axis singularity in the Hankel function $H_0^{(2)}$ at $k_{zr} = k$ and ensures rapid convergence of the integrand for both near-field and far-field evaluations.

in Fig. 1. Purely planar structures are defined as those with height $h = 0$, whereas quasi-planar structures refer to those with a nonzero height $h \neq 0$, regardless of whether h is smaller or larger than the wavelength λ. A quasi-planar structure is thus simply characterized here as a structure with a small height-to-diameter ratio, $h/P_{\max} \ll 1$. We define a cylindrical system of coordinates $(\hat{\boldsymbol{\rho}}, \hat{\boldsymbol{\phi}}, \hat{z})$ and a Cartesian system of coordinates $(\hat{\boldsymbol{x}}, \hat{\boldsymbol{y}}, \hat{z})$. A source point $\mathbf{r}_s = x_s\hat{\boldsymbol{x}} + y_s\hat{\boldsymbol{y}} + z_s\hat{z}$ is represented by the cylindrical coordinates (ρ_s, ϕ_s, z_s), while an observation point $\mathbf{r} = x\hat{\boldsymbol{x}} + y\hat{\boldsymbol{y}} + z\hat{z}$ is denoted by coordinates (ρ, ϕ, z). The distance between these points is given by $R = (P^2 + (z - z_s)^2)^{1/2}$ where the in-plane distance is defined by $P = ((x - x_s)^2 + (y - y_s)^2)^{1/2}$. A group i is enclosed within a cylinder of height h, radius a, and center $\mathbf{r}_i = x_i\hat{\boldsymbol{x}} + y_i\hat{\boldsymbol{y}}$ which lies in the $z = 0$ plane. The in-plane distance P between any pairs of source and observation points ranges from $P_{\min}$ to $P_{\max}$.

We begin with a reminder of the SDM decomposition [26]. This starts with the decomposition of the free-space 3-D Green's function (GF) into a spectrum of 2-D line sources as follows:

$$\begin{aligned} G(k, R) &= \frac{e^{-jkR}}{4\pi R} \\ &= \frac{-j}{8\pi} \int_{-\infty}^{\infty} H_0^{(2)}\left(k_\rho P\right) e^{-jk_z(z-z_s)}\, \mathrm{d}k_z \end{aligned} \tag{1}$$

where k is the wavenumber, k_z and $k_\rho = (k_x^2 + k_y^2)^{1/2} = (k^2 - k_z^2)^{1/2}$ are the vertical and radial spectral components, respectively, of the wavevector $\mathbf{k} = k_x\hat{\boldsymbol{x}} + k_y\hat{\boldsymbol{y}} + k_z\hat{z}$, and $H_0^{(2)}$ is the second-kind Hankel function of zero order. A contour deformation in the complex plane must then be used to avoid numerical issues stemming from the singularity of the Hankel function which appears for $k_{zr} = k$. Since the function $H_0^{(2)}(k_\rho P)$ oscillates as $e^{-jk_{\rho r}P}$, it can be efficiently integrated along the SDP ([44]) where $k_{\rho,r}$ is kept constant, thus removing the modulation. The SDP is illustrated in Fig. 2 and is defined by the following equations:

$$k_{zi} = \frac{k_{zr}}{S} \tag{2}$$

where $S = (1 + (k_{zr}/k)^2)^{1/2}$, and the contour derivative is given by $k'_{zi} = 1/S$. It must be noted that the SDP is not suited to structures with height h much larger than the wavelength because the amplitude of the Hankel function grows significantly in the visible region $k_{zr} \in [-k, k]$ causing large round-off errors [45]. In such cases, a contour with a lower maximum height k_{zi} is preferable.

The next step involves expanding the Hankel function in (1) using Rokhlin's 2-D multipole expansion [14]. For an observation point $\mathbf{r}$ in the group i and a source point $\mathbf{r}_s$ in the group j, we can write

$$\begin{aligned} H_0^{(2)}(k_\rho P) = \frac{1}{2\pi} \int_0^{2\pi} e^{j\mathbf{k}_\rho\cdot(\mathbf{r}-\mathbf{r}_j)}\; & T\left(kP_{ij}, \alpha - \phi_{ij}\right) \\ & \times e^{-j\mathbf{k}_\rho\cdot(\mathbf{r}_s-\mathbf{r}_i)}\, \mathrm{d}\alpha \end{aligned} \tag{3}$$

where P_{ij} and ϕ_{ij} are the polar coordinates of the in-plane relative distance $\boldsymbol{P}_{ij} = \mathbf{r}_j - \mathbf{r}_i$, α represents the azimuthal angle associated with a plane wave with wavevector $\mathbf{k}$, and its horizontal projection is $\mathbf{k}_\rho = k_\rho \cos\alpha\; \hat{\mathbf{x}} + k_\rho \sin\alpha\; \hat{\mathbf{y}}$. The translation function of the 2-D multipole expansion is written as

$$T(k_\rho P_{ij}, \alpha) = \sum_{m=-\infty}^{\infty} j^m\; H_m^{(2)}\left(k_\rho P_{ij}\right) e^{jm\alpha} \tag{4}$$

where $H_m^{(2)}$ is the second-kind Hankel function of order m. Finally, substituting (3) into the line-source decomposition (1) leads to the SDM decomposition of the 3-D GF [26]

$$\begin{aligned} G(k, R) = \frac{-j}{16\pi^2} \int_{-\infty}^{\infty} \int_0^{2\pi} e^{j\mathbf{k}\cdot(\mathbf{r}-\mathbf{r}_j)}\; & T\left(k_\rho P_{ij}, \alpha - \phi_{ij}\right) \\ & \times e^{-j\mathbf{k}\cdot(\mathbf{r}_s-\mathbf{r}_i)}\, \mathrm{d}\alpha\; k'_z \mathrm{d}k_{zr} \end{aligned} \tag{5}$$

where $k'_z = (1 + jk'_{zi})$ accounts for the contour derivative. Expression (5) differs from the 3-D multipole decomposition [14] as it uses the 2-D translation function and integration along the vertical wavenumber k_z. For quasi-planar geometries, it only requires plane waves propagating near the horizontal plane, i.e., at small k_{zr} values. The number of samples along k_{zr} also scales nearly linearly with the horizontal electrical size ka [25], [26], unlike the quadratic scaling $(ka)^2$ in the traditional 3-D multipole expansion. Sampling rules for discretizing (5) at high frequencies are provided in [25].

III. Numerical Challenges at Subwavelength Distances

For small relative distances P_{ij} below half a wavelength, the multipole decomposition (3) becomes inaccurate and the required number of samples along k_{zr} rapidly increases due to the need for more evanescent waves. In this section, we delve deeper into these two numerical challenges. In Section IV, we will present the techniques that lead to the broadband extension of the SDM expansion.

A. LF Breakdown of the Multipole Expansion

The LF breakdown of the multipole decomposition is a well-known numerical issue [28], [35] that arises when the translation function in (3) is evaluated at a small argument kP_{ij}, i.e., at low frequencies and/or small distances. The ill-conditioning results from an attempt to evaluate reactive near fields, with spatial spectrum extending far beyond the visible domain, using only far-field information. Mathematically, the breakdown is attributed to the overexponential asymptotic growth of the Hankel functions $H_m^{(2)}$ with respect to order m in (4) for small arguments $|k_\rho P_{ij}| < m$ [46]

$$H_m^{(2)}\left(k_\rho P_{ij}\right) \approx \frac{-j}{\pi}\ (m-1)!\ 2^m\ \left(k_\rho P_{ij}\right)^{-m} \tag{6}$$

where $(m-1)!$ is the asymptotically dominant function. Despite their similar importance to overall accuracy, the low-order terms in (4) have much smaller amplitudes compared with the higher order ones. For instance, when $M = 10$, $k_\rho = k$, and $P_{ij} = 0.1\lambda$, we have $|H_M^{(2)}(k_\rho P_{ij})/H_0^{(2)}(k_\rho P_{ij})| \approx 10^{10}$. Due to finite machine precision, the amplitude of low-order terms can be smaller than the round-off noise of higher order terms, leading to numerical breakdown.

B. Wide Evanescent Spectrum

The second numerical issue is related to the computation of the outer integral along k_{zr}. For simplicity, we can focus solely on the line-source decomposition (1) and consider the in-plane case $z - z_s = 0$. The integrand is then decaying exponentially at large k_{zr} values for which $k_\rho \approx jk_{zi}$. Using the large-argument approximation of $H_0^{(2)}(x)$ [46], the relative truncation error is estimated as

$$\begin{aligned}\epsilon &\approx \sqrt{2P/\pi}\int_{k_{zm}}^{\infty}\frac{e^{-k_{zr}P}}{\sqrt{k_{zr}}}\,\mathrm{d}k_{zr}\\ &= \sqrt{2}\ \operatorname{erfc}\left(\sqrt{k_{zm}P}\right)\end{aligned} \tag{7}$$

where erfc is the complementary error function, and k_{zm} is the truncation limit. Using $\operatorname{erfc}(x) < e^{-x^2}$, we obtain a bound for k_{zm}

$$k_{zm} \gtrsim \frac{-\ln\left(\epsilon/\sqrt{2}\right)}{P}. \tag{8}$$

On one hand, the truncation limit k_{zm} must increase as the distance P decreases to account for the more singular behavior of the GF by including higher spatial frequencies. For instance, for a target error level of $\epsilon = 10^{-2}$ and $P = 0.01\lambda$, the integration must be performed up to $k_{zm} \sim 80\ k$, far beyond the visible limit which is located at $k_{zr} = k$. On the other hand, the sampling step Δk used to discretize (1) must decrease linearly with increasing distance P as result of the Gaussian decay of $H_0^{(2)}$ along the SDP at low k_{zr}. To devise an efficient expansion, the evaluation of (1) with a given Δk and k_{zm} must remain accurate for a range of distances P covering the entire observation domain, i.e., with $P \in [P_{\min}, P_{\max}]$. For instance, when $P_{\min} = 0.01\lambda$ and $P_{\max} = 10\lambda$, this approach would require thousands of samples along k_{zr}.

IV. Broadband SDM Formulation

We now present a broadband SDM decomposition of the GF, addressing the two numerical issues previously described. First, we resolve the LF breakdown of the 2-D multipole decomposition using a renormalization approach similar to [28], [40], and [41], but we retain the plane-wave formulation instead of using azimuthal harmonics. Second, we tackle the challenge of the extensive evanescent spectrum through nonuniform sampling. Finally, we validate the multipole expansion of the 3-D GF function with numerical experiments.

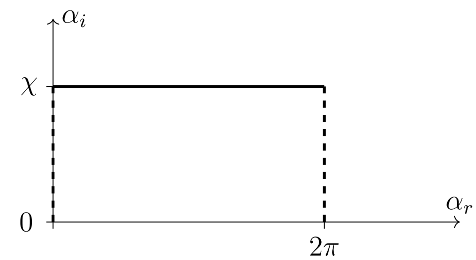

Fig. 3. Depiction of the complex azimuthal integration path with a constant shift χ. The path modification stabilizes the multipole expansion by counteracting the overexponential growth of high-order terms in the translation function T_o, ensuring accurate evaluation for small subwavelength distances P_{ij}.

A. Stabilitization of the Multipole Expansion

Let us first define the one-sided translation function, which includes only the positive orders of the translation function T, as follows:

$$T_o(kP_{ij},\alpha) = \sum_{m=0}^{\infty} c_m\ j^m\ H_m^{(2)}\left(kP_{ij}\right)\ e^{jm\alpha} \tag{9}$$

where $c_m = 1/2$ for $m = 0$ and $c_m = 1$ otherwise. Observing the relation $T(kP_{ij},\alpha) = T_o(kP_{ij},\alpha) + T_o(kP_{ij},-\alpha)$, we can then rewrite the decomposition (3) of the Hankel function into two terms

$$H_0^{(2)}(kP) = H_+(kP) + H_-(kP) \tag{10}$$

where $H_\pm$ are functions obtained by evaluating the multipole decomposition with the one-sided translation function T_o

$$H_\pm(kP) = \int_0^{2\pi} e^{j\mathbf{k}_\rho\cdot(\boldsymbol{\rho}-\mathbf{r}_j)}\,T_o\left(kP_{ij},\pm\left(\alpha-\phi_{ij}\right)\right)e^{-j\mathbf{k}_\rho\cdot(\boldsymbol{\rho}_s-\mathbf{r}_i)}\ \mathrm{d}\alpha. \tag{11}$$

This splitting over the indices m of the translation function T is equivalent to that performed over the indices k in (12) and (14) in [40]. As outlined in [35], we deform the integration path along the azimuthal angle α to a contour in the complex plane with three segments: one horizontal segment parallel to the real axis with shift $\alpha_i = \pm\chi$ for $H_\pm$, respectively, and two vertical segments parallel to the imaginary axis at $\alpha_r = 0$ and $\alpha_r = 2\pi$, as depicted in Fig. 3 for H_+. Since the integrand is 2π-periodic, the contributions along the two vertical branches cancel out, leaving only the horizontal segment. Evaluating the one-sided translation function at $\alpha = \pm\alpha_r + j\chi$ produces a decreasing exponential factor $e^{-m\chi}$ as a function of order m

$$T_o(kP,\alpha) = \sum_{m=0}^{\infty} c_m\ j^m\ H_m^{(2)}(kP)\ e^{-m\chi}\ e^{\pm jm\alpha_r}. \tag{12}$$

The exponential factor $e^{-m\chi}$ counteracts the factorial increase (6) of $H_m^{(2)}$, thereby renormalizing the amplitude of each term. When the sum in (12) is truncated to a maximum order M, the complex shift χ can be chosen such that the ratio between the highest order ($m = M$) and lowest order ($m = 0$) Hankel functions in the translation function is balanced by the exponential

$$\chi(k) = \frac{1}{M} \log \frac{\left| H_M^{(2)}(kP_{\min}) \right|}{\left| H_0^{(2)}(kP_{\min}) \right|} \tag{13}$$

where the dependency of χ on k is introduced, as we will simply replace k with the complex value k_ρ when using this formula for the 3-D expansion.

B. Nonuniform Sampling Along the Vertical Wavenumber k_{zr}

As discussed in Section III-B, the required number of plane waves with uniform sampling along k_{zr} becomes prohibitively high for observation domains with small distances $P_{\min}$ because the truncation limit k_{zm} increases substantially while the step size Δk is still constrained by the variation in $H_0^{(2)}$ at the largest distance $P_{\max}$. To address this, we adopt a nonuniform sampling along k_{zr} with a step size Δk that increases linearly with k_{zr}. This is motivated by the observation [42] that plane waves with larger k_{zr} values contribute significantly only at smaller distances P, for which $H_0^{(2)}$ is decaying at a slower rate. According to [25], the nonuniform sampling can be implemented using the following change in variables:

$$s_{zr} = \operatorname{asinh}(bk_{zr})/b \tag{14}$$

where asinh is the inverse hyperbolic sine, b is a parameter, and $\mathrm{d}k_{zr}/\mathrm{d}s_{zr} = \cosh(bs_{zr})$ is the Jacobian of the transformation. When $bk_{zr} \gg 1$, the sampling along k_{zr} is almost regular since we have $s_{zr} \simeq k_{zr}$. For larger s_{zr}, the sampling increases exponentially [42], with $k_{zr} \simeq 1/(2b)e^{bs_{zr}}$. As highlighted in (7), at large k_{zr}, the Hankel function behaves as a decaying exponential. Therefore, the exponential sampling is designed to counteract this exponential decay

$$e^{-k_{zr}P} \sim e^{-P/(2b)e^{bs_{zr}}}. \tag{15}$$

As illustrated in Fig. 4, without the change in variable, the amplitude Fig. 4(a) of the Hankel function decays sharply with respect to k_{zr} and contracts rapidly with P, while the phase Fig. 4(b), wrapped from $-\pi$ to π, exhibits significant variation at small k_{zr}. After the change in variable, both the amplitude Fig. 4(c) and phase Fig. 4(d) become smoother with respect to s_{zr} and vary less with P, enabling integration with fewer points.

Following [25], the new variable s_{zr} can be sampled on a grid with spacing Δs and truncation limit s_{zm} given by

$$\begin{aligned} \Delta s &= \pi\left(-k/\left(P_{\max} \ln \epsilon\right)\right)^{1/2} \\ s_{zm} &= \operatorname{asinh}\left(bk_{zm}\right)/b. \end{aligned} \tag{16}$$

For purely planar cases ($h = 0$), we can select $b = \pi/(-\ln \epsilon \Delta s)$ and k_{zm} with (8). The number of samples N_z now scales with [25]

$$N_z = \frac{2s_{zm}}{\Delta s} \propto -\ln \epsilon \;\; \ln \frac{P_{\max}}{P_{\min}} \tag{17}$$

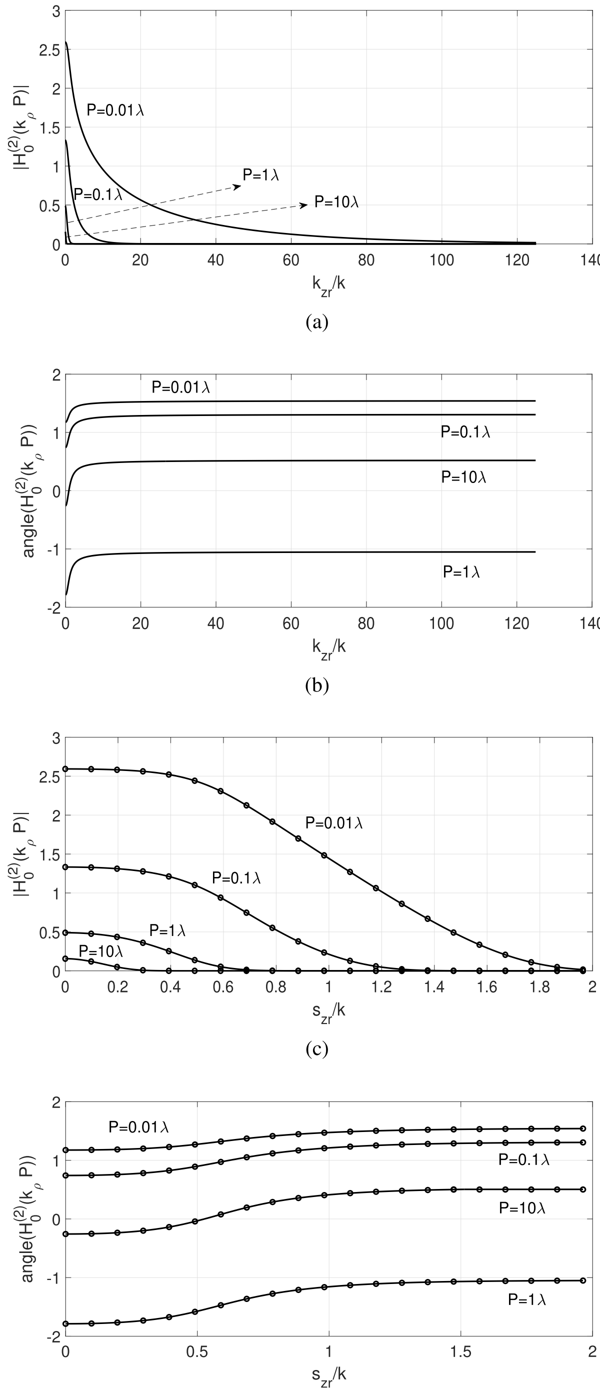

Fig. 4. Amplitude (a) and phase (b) of the Hankel function $H_0^{(2)}$ along the SDP without the transformation in (14) for distances $P = \{0.01, 0.1, 1, 10\}\lambda$. (b) Amplitude and (c) phase of $H_0^{(2)}$ after applying the transformation in (14), showing reduced variation with distance P and increased smoothness with respect to s_{zr}. For a target error $\epsilon = 10^{-4}$, we have $k_{zm}/k = 125$, $\Delta s/k = 0.1$, $b = 1.31$, and $N_z = 21$. These results highlight the effectiveness of the nonuniform sampling approach along k_z for handling a wide range of distances P.

instead of being inversely proportional to $P_{\min}$ as with regular sampling. For $\epsilon = 10^{-4}$, we have $k_{zm}/k = 125$, $\Delta s/k = 0.1$, and $b = 1.31$, and this approach only requires $N_z = 21$ samples. For nonplanar structure ($h > 0$), the oscillation with $z - z_s$ in (1) must be considered. To prevent the sampling from exceeding the Nyquist rate π/h near the end of the integration of the integration domain, a slightly lower value of b can be chosen with the following rule of thumb:

$$b \sim \min\left(\frac{\pi}{-\ln \epsilon \Delta s}, \frac{\gamma \pi}{k_{zm} h \Delta s}\right) \tag{18}$$

where $\gamma \simeq 1$ is manually adjusted. The truncation limit k_{zm} can be selected with (8) but the target error level ϵ must be multiplied with e^{hk} to account for the exponential increase $e^{k_{zi}(z-z_s)}$ of the integrand in (1) along the SDP.

C. Numerical Evaluation of the 3-D GF

We can now analyze the 3-D problem by substituting the expansion (10) of $H_0^{(2)}$ into (1), along with the transformation (14) and the two contour deformations. Discretizing both the integrals leads to

$$G(k, R) = G_+(k, R) + G_-(k, R) \tag{19}$$

with

$$G_\pm(k, R) = \sum_{p=1}^{N_s} \sum_{n=0}^{2M} w_p T_o\big(k_{\rho,p} P_{ij}, \pm(\alpha_{r,n} - \phi_{ij}) + j\chi_p\big) \times e^{j\mathbf{k}_{pn}\cdot(\mathbf{r}-\mathbf{r}_j)}\ e^{-j\mathbf{k}_{pn}\cdot(\mathbf{r}_s-\mathbf{r}_i)} \tag{20}$$

where the wavevector of the plane wave pn is $\mathbf{k}_{pn} = k_{\rho,p}\cos\alpha_n\hat{\mathbf{x}} + k_{\rho,p}\sin\alpha_n\hat{\mathbf{y}} + k_{z,p}\hat{z}$, the integration weight is $w_p = k'_{z,p}\cosh(bs_{zr,p})\Delta s$, and the contour shift is $\chi_p = \chi(k_{\rho,p})$ according to (13).

First, we validate the numerical evaluation of the GF through a purely planar experiment ($h = 0$) where the source group size a increases from electrically small ($a = 0.001\lambda$) to electrically large ($a = 25\lambda$). The minimum distance between source and observation domains increases with the group size as $P_{\min} = a$. The maximum distance is fixed at $P_{\max} = 50\lambda$. As shown in Fig. 5(a), we achieve error levels $\epsilon = \{10^{-2}, 10^{-4}, 10^{-6}\}$ across the full frequency range, confirming that our representation is broadband and stable at very low frequencies. The truncation order M of the translation function and the number N_z of samples along k_{zr} are analyzed in Fig. 5(b). The order M is kept constant in the LF regime and progressively converges to the excess bandwidth formula [39], i.e., increasing linearly with a/λ. The number N_z increases with $-\ln P_{\min}$, as predicted. The bump around $a/\lambda = 1$, in the intermediate-frequency range of the error curves, is simply due to the transition from the LF sampling rules to the HF rules derived in [25] and can be accommodated by choosing a slightly higher target error level.

Second, we propose a nonplanar experiment and analyze the variation in the maximum error with N_z and M at the minimum distance $P_{\min}$. To be representative of typical 3-D antenna sizes, we consider a cylinder of fixed height $h = \lambda/3$ and group size $a = \lambda/6$. The maximum distance is set to $P_{\max} = 50\lambda$. The minimum distance ranges $P_{\min}$ from 0.5λ to 0.05λ. As shown in Fig. 6(a), increasing the multipole order M helps decrease the error at the smallest distance, with $M = 30$ leading to an error of 10^{-2} and $M = 50$ to an error of 10^{-4}. One can see in Fig. 6(b) that for these minimum distances $P_{\min}$, the number of samples N_z remains reasonable between 10 and 100. The minimum distance of 0.05λ considered here is an order of magnitude lower than where the classical multipole expansion breaks down, which is around 0.5λ, as shown later in Fig. 7.

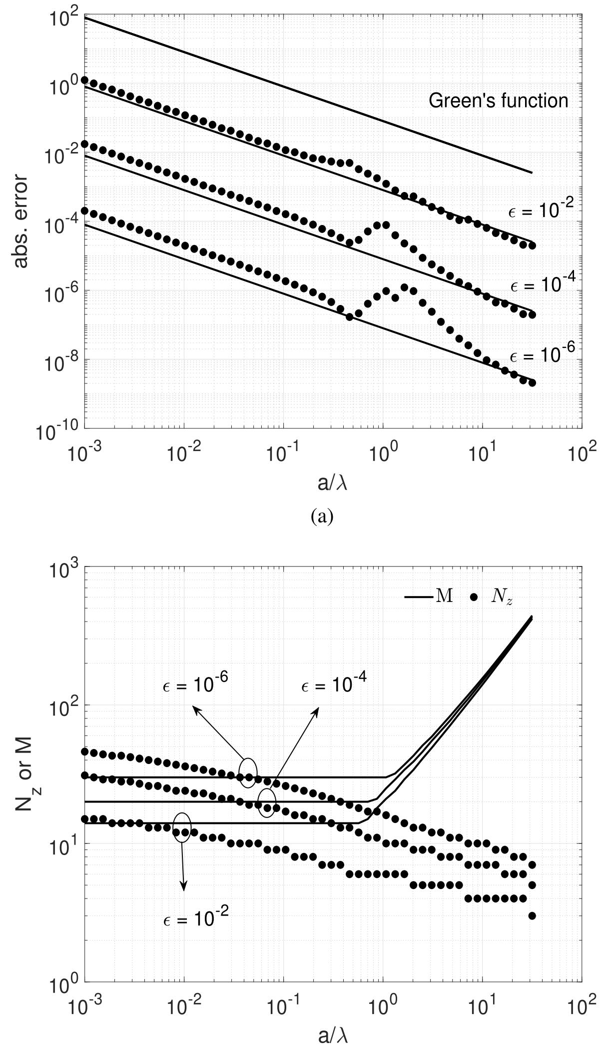

(a) (b)

Fig. 5. (a) Maximum absolute errors in the 3-D GF evaluation for a planar scenario ($h = 0$) as the group size a/λ increases, with $P_{\min} = a$ and $P_{\max} = 50\lambda$. Error levels $\epsilon = \{10^{-2}, 10^{-4}, 10^{-6}\}$ demonstrate the method's broadband stability. (b) Number of samples N_z and truncation order M required for convergence, illustrating the efficiency of the proposed approach.

V. Accelerated MoM Solver

In this section, we apply the SDM decomposition for the rapid evaluation of mutual MoM interactions. We begin with a brief overview of the MoM system of equations and the MBF framework. Then, we introduce the SDM formulation of the MoM interactions and demonstrate how to recompute these interactions for rotated antennas. Finally, we validate the method with a numerical test involving two log-periodic antennas.

A. Reminder on the MoM-MBF Framework

Assuming an array of N_a disconnected antennas, the MoM impedance matrix $\mathbf{Z}$, the excitation vector $\mathbf{v}$, and the unknown coefficients $\mathbf{x}$ can be partitioned into per-antenna blocks,

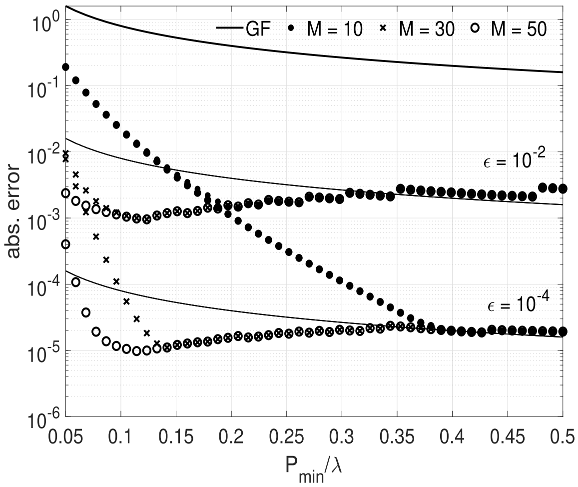

(a)

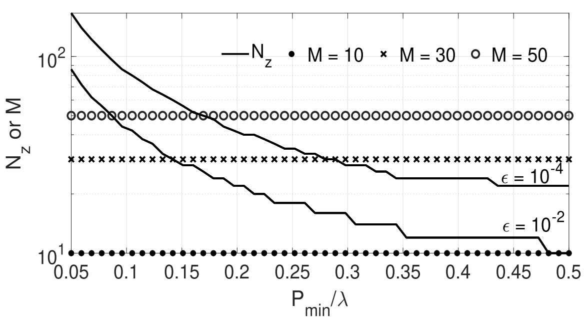

(b)

Fig. 6. (a) Maximum absolute errors in the 3-D GF evaluation for a nonplanar scenario ($h = \lambda/3$) with fixed group size $a = \lambda/6$ and $P_{\max} = 50\lambda$. The minimum distance $P_{\min}$ varies from 0.05 to 0.5λ. (b) Number of samples N_Z and truncation order M required for convergence to error level $\epsilon = \{10^{-2}, 10^{-4}\}$, illustrating the efficiency of the method in evaluating mutual interactions within nonplanar structures at close subwavelength distances.

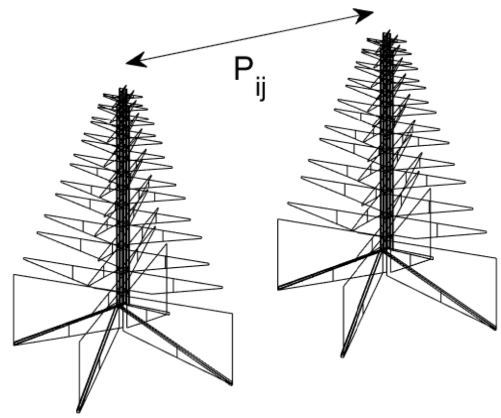

(a)

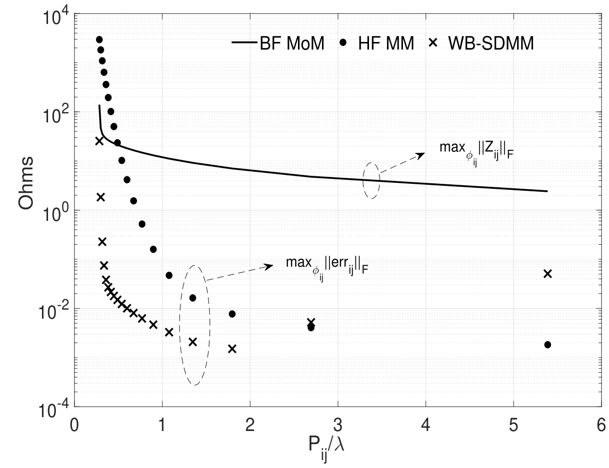

(b)

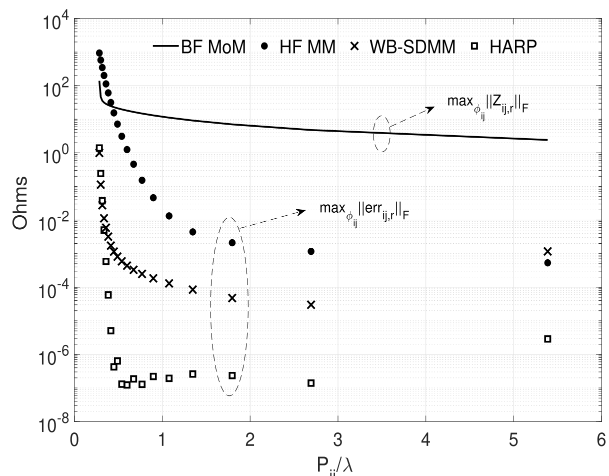

(c)

Fig. 7. (a) Experimental setup for evaluating MoM mutual interactions between two SKALA4 antennas. (b) Maximum Frobenius norm errors for mutual interactions between elementary basis functions using BF MoM, HF-MM, WB-SDMM, and HARP. (c) Comparison of Frobenius norm errors for interactions between 50 MBFs, demonstrating the accuracy of WB-SDMM at short baseline lengths.

leading to the following system of equations:

$$\begin{bmatrix} \mathbf{Z}_{11} & \dots & \mathbf{Z}_{1N_a} \\ \vdots & \vdots & \vdots \\ \mathbf{Z}_{N_a1} & \dots & \mathbf{Z}_{N_aN_a} \end{bmatrix} \begin{bmatrix} \mathbf{x}_1 \\ \vdots \\ \mathbf{x}_{N_a} \end{bmatrix} = \begin{bmatrix} \mathbf{v}_1 \\ \vdots \\ \mathbf{v}_{N_a} \end{bmatrix} \tag{21}$$

where a block $\mathbf{Z}_{ii}$ on the diagonal corresponds the self-interaction matrix of antenna i while an off-diagonal block $\mathbf{Z}_{ij}$ contains mutual interactions between basis functions on antenna i and j. For a perfectly electrically conducting scatterer, an MoM system of equations is derived from the electric field integral equations using Galerkin testing. The entry mn of the block $\mathbf{Z}_{ij}$ corresponds to the integral reaction between testing function $\mathbf{f}_m$ on antenna i and basis function $\mathbf{f}_n$ on antenna j. It is given by

$$\left[\mathbf{Z}_{ij}\right]_{mn} = \int\int_{S_m \times S_n} \mathbf{f}_m(\mathbf{r}) \cdot \mathbf{G}\left(k, \mathbf{r}, \mathbf{r}_s\right) \cdot \mathbf{f}_n\left(\mathbf{r}_s\right) \, \mathrm{d}S_m \mathrm{d}S_n \tag{22}$$

where $\mathbf{G}$ is the dyadic GF describing the interaction between points $\mathbf{r}$ and $\mathbf{r}_s$ on the surfaces S_m and S_n, respectively.

For a large number of basis functions per antenna, filling and inverting the matrix $\mathbf{Z}$ become prohibitively costly even for a small number of antennas. The inversion step can be accelerated using a reduced set of macro-level basis (MBF, [22]) functions defined on the entire antenna surface and expressed as linear combinations of elementary basis functions, $\mathbf{x}_i \approx \mathbf{Q}\mathbf{x}_{r,i}$, with the matrix $\mathbf{Q}$ containing precomputed MBF coefficients. This yields a reduced system of equations with the size of the reduced matrix $\mathbf{Z}_{r,ij} = \mathbf{Q}^H \mathbf{Z}_{ij} \mathbf{Q}$ being much smaller than that of the original matrix $\mathbf{Z}_{ij}$. A challenge remains in constructing the reduced matrices $\mathbf{Z}_{r,ij}$ without fully evaluating all elementary blocks $\mathbf{Z}_{ij}$ beforehand. An initial 3-D multipole method was proposed in [20], but it is not suitable for short distances. Another method, HARP [17], maintains accuracy at short distances. Assuming the same set of MBFs for each antenna, it models MBF interactions using an HARP function, with coefficients derived from a reduced set of elementary blocks $\mathbf{Z}_{ij}$ tabulated on a radial-azimuthal nonuniform grid [19]. As demonstrated later, precomputing these elementary blocks can become costly for antennas with many elementary basis functions. In addition, it does not allow the presence of rotated antennas in the array. In Section V-B, we will instead build on the first approach [20] and replace the HF multipole method with the SDM-based approach developed in this article.

B. Rapid Evaluation of Mutual Interactions Using the Broadband SDM Decomposition

The derivation of the multipole-based MoM interaction is achieved by substituting the GF decomposition in (22) and interchanging spatial and spectral integrations, and then reexpressing spatial derivatives as products in the spectral domain [26], [47]. Similar to Section IV-C, the broadband formulation requires splitting the interactions into two terms,

$$\left[\mathbf{Z}_{ij}\right]_{mn} = \left[\mathbf{Z}_{ij}\right]_{mn,+} + \left[\mathbf{Z}_{ij}\right]_{mn,-} \tag{23}$$

with

$$\left[\mathbf{Z}_{ij}\right]_{mn,\pm} = \frac{1}{k\eta} \int_{-\infty}^{\infty} \int_{0}^{2\pi} \mathbf{p}_m\big(-k_z, \alpha + \pi\big) \cdot \mathbf{p}_n\big(k_z, \alpha\big) \times T_o\big(k_\rho P_{ij}, \pm(\alpha_r - \phi_{ij}) + j\chi\big)\, \mathrm{d}\alpha_r\ k_z' \mathrm{d}k_{zr} \tag{24}$$

where the complex pattern of basis function m is given by $\mathbf{p}_m = \eta/(2j\lambda)(\tilde{\mathbf{f}}_m - (\tilde{\mathbf{f}}_m \cdot \mathbf{k})\ \mathbf{k}/k^2)$ with the Fourier spectrum $\tilde{\mathbf{f}}_m$ defined in (28). Expanding the pattern product into TE–TM components leads to

$$\mathbf{p}_m \cdot \mathbf{p}_n = p_{m,TE} \cdot p_{n,TE} + p_{m,TM} \cdot p_{n,TM}. \tag{25}$$

For identical antennas, this product is independent of baseline and therefore can be precomputed for all pairs of MBFs and stored prior to matrix filling.

If each antenna i is now rotated by an angle β_i, the pattern product (25) needs to be recalculated for each antenna pair, resulting in a slight increase in computational cost, as demonstrated later in Section VI-B. To facilitate this rotation, we expand each pattern using azimuthal harmonics

$$p_{m,q}(k_z, \alpha) = \sum_{l=-M/2}^{M/2} c_{ml,q}(k_z)\ e^{jl\alpha_z}. \tag{26}$$

Here, $c_{ml,q}$ are the harmonic coefficients for TE and TM modes, and the expansion is truncated to $\pm M$. Details on obtaining these coefficients directly from the basis function $\mathbf{f}_m$ are provided in Appendix . When antennas are rotated, (26) is simply updated by replacing α with $\alpha - \beta_i$.

We now validate the formulation using a single-baseline experiment involving two wideband log-periodic antennas, each standing 2 m tall and 1.6 m in diameter. This antenna, known as SKALA4 [10] and shown in Fig. 7(a), is representative of those used in the square kilometer array telescope [48]. The simulations are carried out at a frequency of 50 MHz, which is at the lower end of the operating band. Each antenna is meshed with approximately 3600 basis functions. The minimum relative distance between the centers of the antennas is 1.7 m (0.3 wavelengths). When the dipoles of two antennas are aligned, the closest distance between metallizations is 0.1 m, equivalent to 0.015 wavelengths. The baseline angle is varied from 0 to 2π. The experimental setup is illustrated in Fig. 7(a).

We compute the absolute errors between elementary interactions using the BF MoM method, the wideband SDM method (WB-SDMM) with $N_z = 30$ and $M = 30$, and the classical high-frequency 3-D multipole method (HF-MM) with $M = 10$. These errors are measured as the Frobenius norm of the difference with the BF MoM blocks. Maximum error values across all baseline angles are plotted for a given baseline length in Fig. 7(b). It is clear that the HF-MM method quickly deteriorates for distances smaller than a wavelength, whereas the WB-SDMM remains accurate, achieving one-digit accuracy at the smallest distance. In Fig. 7(c), we compare the same errors for MBF interactions, this time including HARP with 30 radial points and 60 azimuthal points to parameterize the interaction model. The number of MBFs is 50. While HARP shows slightly lower errors at intermediate and larger distances, the WB-SDMM does slightly better at small distances. The worst case error for MBF interactions is two digits of accuracy, which is one order less than for elementary interactions. The computation times per MBF interaction for both HARP and WB-SDMM were on the order of one-tenth of a millisecond on a laptop, demonstrating similar accuracy within comparable runtime.

VI. Numerical Examples

We now examine three different arrays and analyze computation costs and memory requirements. The simulations run on a laptop equipped with an Intel Core i7-13800H processor (2.50 GHz, 14 cores) and 32.0 GB of RAM. In these examples, we consider the dual-polarized SKALA4 antenna [10], shown in Fig. 7(a), each loaded with a 100-Ω resistor and operating between 50 and 350 MHz. The antenna is modeled using wire segments and around 3600 wire basis functions, with the MoM using the thin-wire Pocklington approximation. The mutual interactions between elementary basis functions are computed in C++, though this computation is not parallelized. This in-house code has been validated against multiple commercial solvers in [17] and [25]. The antenna self-interaction elementary block $\mathbf{Z}_{ii}$ varies smoothly with frequency. Therefore, these can be computed and stored beforehand on a very coarse grid and subsequently rapidly interpolated at a finer frequency resolution in less than a second. For all the simulations, the number of MBFs is fixed to one primary and 50 secondary MBFs and we aim to compute all the EEPs for each antenna and for both the feeds. The EM simulator developed in this article is named fast array simulation tool (FAST).

A. Array of 256 Randomly Placed Log-Periodic Antennas

In this example, we consider an irregular array of 256 SKALA4 antennas positioned in a pseudorandom manner [see the right-side array layout in Fig. 11(a)]. The minimum and maximum baseline lengths in this layout are 1.75 and 38 m, respectively. First, we benchmark FAST and validate it against FEKO's MLFMM solver [43]. Note that FEKO runs on a large workstation with 128 cores and 2 TB of RAM and uses the MLFMM solver with a sparse LU preconditioner. The iterative solver converges in between 10 and 20 iterations for each EEP. We also compute the EEPs with HARP using radial and azimuthal orders $N = 10$ and $M = 10$. FAST is parameterized with $N_z = 14$ and $M = 10$. Fig. 8(a) shows the EEP of an element near the edge of the array. The errors of FAST with respect to FEKO (left) and HARP (right) are shown in Fig. 8(b) and (c), respectively. The agreement with FEKO is around -25 dBV, while with HARP it is around -35 dBV, which corresponds to almost two digits of accuracy in the electric far-field.

The computation times and peak memory usage are summarized in Table I. The preparation time for FAST is about 100× faster than for HARP. Moreover, FAST running on a laptop outperforms FEKO's MLFMM on a 128-core workstation by a factor of 25 in total run time. Both FAST and HARP use only 3.7 GB of RAM, which is significantly less than the 350 GB required by the MLFMM. Modifying the array layout with HARP and FAST involves only refilling and resolving the reduced MoM matrix, taking approximately one additional minute. In contrast, the MLFMM requires a complete restart, consuming an additional 4 h. Regarding precomputations, HARP spends most of its time computing elementary blocks for MBF generation and HARP model parameterization, requiring 50 and 200 MoM blocks, respectively, each taking under 6 min on a laptop. In comparison, FAST takes around 10 s to generate one MBF and its complex pattern. Reduced matrix filling takes about 12 s for HARP and 14 s for FAST. Solving the $12\,800 \times 12\,800$ reduced MoM matrix takes 30 s for both the methods. In conclusion, FAST's precomputation steps are around two orders of magnitude faster than HARP's, while both the methods have comparable times for recomputation with a new layout. This speed-up may, however, vary depending on the number of basis functions per antennas.

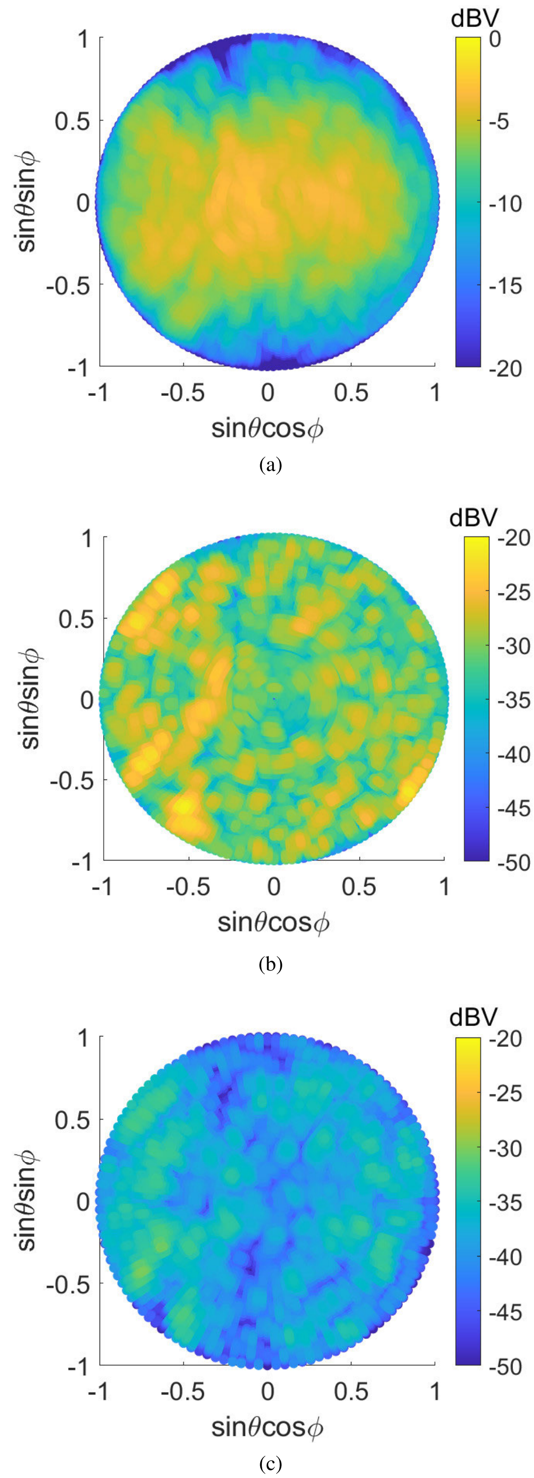

Fig. 8. Example A: (a) EEP in dBV for an edge element (marked with a squared cross in Fig. 11) in the pseudorandom array obtained using the FAST tool. (b) Absolute errors in the far-field pattern compared with FEKO's MLFMM solution, showing agreement within -25 dBV. (c) Absolute errors compared with HARP's solution, achieving an accuracy of -35 dBV.

B. Regular Array of 256 Randomly Rotated Antennas

For rotated antennas, we use the same set of MBFs as in the unrotated configuration. To validate this assumption, we conducted a small example with a 3×3 regular array with a 2.1-m interelement distance, simulated at 125 MHz. As shown in Fig. 9, FAST achieves agreement with the BF MoM method down to approximately -75 dBV in the electric far-field, indicating almost four-digit agreement.

We will now extend the study to a larger array with 16×16 elements. Cuts of the 256 EEPs for feed X in the Y plane are depicted in Fig. 10(a). One immediately notes a significant drop of power around zenith. This effect has been evidenced in simulations in [3] and [49] and results from destructive interference from coupled elements in the regular layout. One way to mitigate this effect is to randomly perturb the antenna positions [49]. Another mitigation approach involves individually rotating each antenna by a random angle

TABLE I

SUMMARY OF COMPUTATION COSTS FOR THE NUMERICAL EXAMPLES

Solver	MLFMM (FEKO)	HARP	FAST		
Machine	AMD EPYC 7662, 128 cores, 1496 MHz, 2TB RAM	Intel Core i7-13800H, 2.50 GHz, 14 cores, 32.0 GB RAM			
Array configuration	256 random			256 regular, rotated	2 x 256 random
Pre-comput. time (mins)	21	1313	10.1	10.1	10.5
Matrix filling time (mins)	-	0.2	0.23	0.5	1.0
Solve time (mins)	230	0.51	0.51	0.51	5.9
Total time (mins)	251	1314	10.8	11.1	17.4
Re-comput. time per new layout (mins)	251	0.71	0.74	1.01	6.9
Peak Memory (GBs)	359	1.3	1.3	1.3	5.3

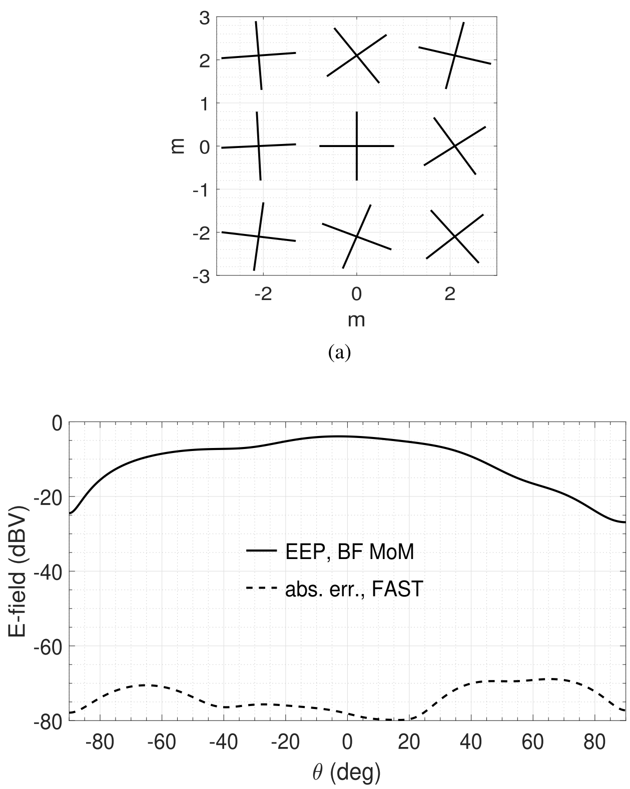

(a)

(b)

Fig. 9. Example B: (a) Experimental setup showing validation of the FAST tool against the BF MoM for a 3 × 3 regular array of rotated antennas with 2.14 m interelement distance at 125 MHz. (b) EEP cross section in the X plane, demonstrating three to four digits of agreement in the electric far-field between FAST and BF MoM simulations.

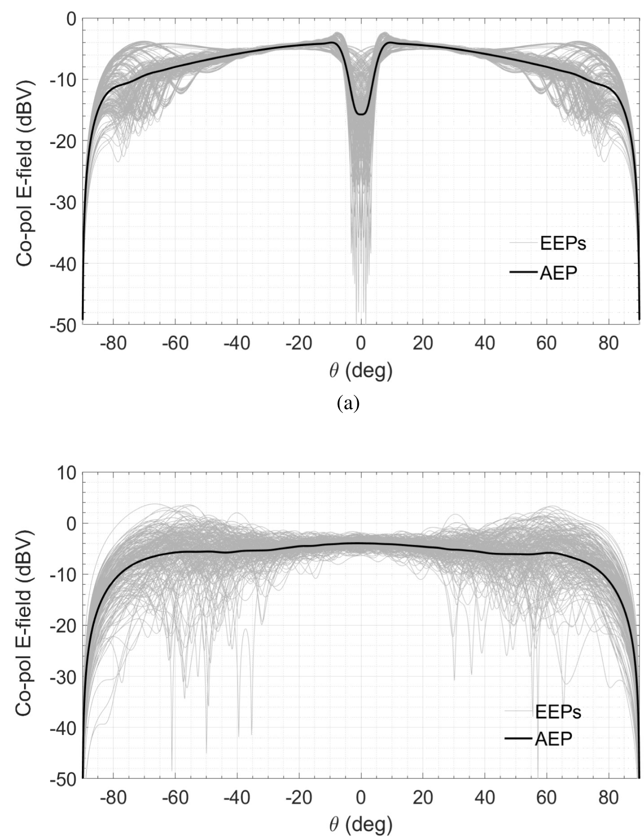

(a)

(b)

Fig. 10. Example B: (a) EEPs (X-feed) in the Y plane for a regular 16 × 16 array with 2.14-m interelement separation at 125 MHz, without random antenna rotations. (b) EEPs with random antenna rotations, demonstrating the mitigation of the zenith null.

while maintaining the layout unchanged. With this strategy, the received voltages from the antennas must be back-rotated in postprocessing to align antenna polarizations

$$\begin{bmatrix} v_{X,i} \\ v_{Y,i} \end{bmatrix} = \begin{bmatrix} \cos\beta_i & -\sin\beta_i \\ \sin\beta_i & \cos\beta_i \end{bmatrix} \begin{bmatrix} v_{X_i,i} \\ v_{Y_i,i} \end{bmatrix} \tag{27}$$

where indices X_i and Y_i refer to antenna i's rotated feed orientations, while X and Y refer to the fixed reference axes. As shown in Fig. 10(b), the dip in the Y plane of the back-rotated EEPs has disappeared, albeit with an increase in variance between elements. Further investigations are necessary to ensure that this correction does not introduce spurious features elsewhere in the frequency band or across the field of view. This design issue is beyond the scope of this analysis article.

The computation times for this example are summarized in Table I. It is noted that compared with the unrotated case, the matrix filling step takes 2× longer due to the need to re-evaluate the pattern product (25) for each baseline.

C. Two Adjacent Stations of the SKA-Low Telescope

The final example involves simulating two closely located phased arrays, called stations, of the LF SKA telescope

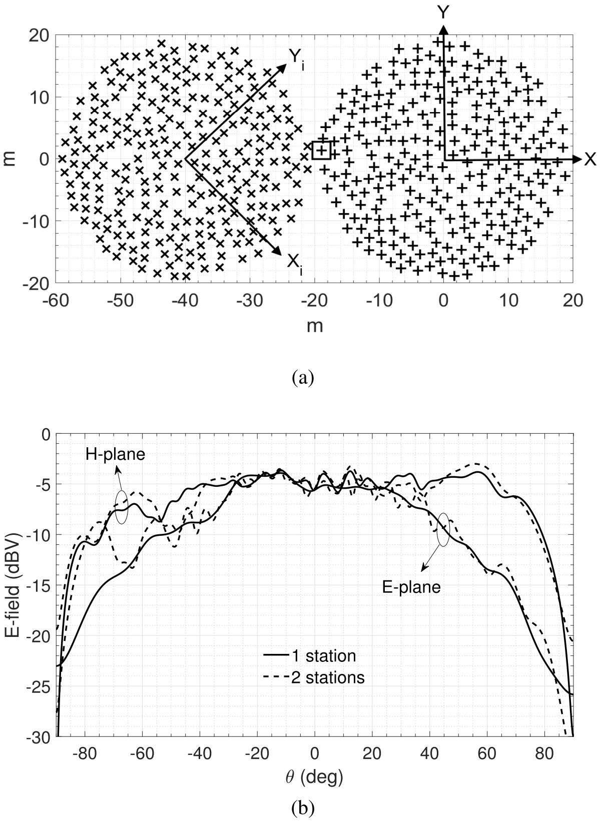

Fig. 11. Example C: (a) configuration showing two closely spaced SKA-low stations with a random layout, where the left-hand station is rotated by 45°. (b) EEP (X-feed) in the E and H–planes at 125 MHz for the edge antenna element (marked with a square) with and without the presence of the second nearby station.

(SKA-low, [48]). In the core of the telescope, stations are densely packed, with minimum distances between them comparable to those within a single array. A devised design approach for SKA-low design is to rotate each of the 512 stations by a given angle varying from 0 to 2π. Considering the same random array layout as in Example A, the scenario is illustrated in Fig. 11. The simulation frequency is set at 125 MHz. The EEP for an edge element (squared) is plotted and compared with that of Example A, which included only the right-hand side station. Significant deviations in the EEP near the horizon and more pronounced ripples are observed. Regarding computation times, this case is a hybrid between Examples A and B, as antennas within a station are not rotated relative to each other, but there is a single relative rotation angle between the stations. The two pattern products, with and without this relative rotation, can be precomputed beforehand. Consequently, the filling time is not increased compared with an equivalent unrotated scenario.

VII. Conclusion

This article introduces a numerical method for analyzing MC effects in large, dense, and irregular arrays of identical antennas, each with potentially thousands of basic functions. The method leverages the MoM with an MBF approach for rapid direct inversion of the MoM impedance matrix and an SDM method (SDMM) to accelerate the matrix filling step. Key advancements include the following.

1) *Broadband SDMM:* We have introduced a stable and efficient broadband expansion for quasi-planar problems, covering low to high frequencies. This approach combines SDP integration on the vertical axis with a 2-D multipole decomposition. It is more efficient than classical 3-D multipole methods at high frequencies, requiring only plane waves propagating near the horizontal plane. Stabilization at low frequencies is achieved with an imaginary shift in the angular integral, and efficiency is further improved by reducing the number of required evanescent waves through a nonuniform sampling scheme. To the author's knowledge, this is the first stable and efficient multipole-based expansion presented for quasi-planar structures.
2) *Low Precomputation Costs:* The SDMM requires only the precomputation of each MBF's complex patterns, resulting in lower antenna-dependent preprocessing costs compared with existing techniques. This is particularly crucial in case of wideband antennas meshed with many elementary basis functions.
3) *Support for Rotated Antennas:* The method accommodates arrays with arbitrarily rotated antennas without incurring significant additional computational cost, offering flexibility for practical applications where antenna orientation may vary.

The proposed method is specifically tailored for the numerical analysis of MC in antenna arrays composed of identical but complex antennas. By precomputing antenna-dependent scattering quantities, such as complex radiation patterns and self-impedance matrices, it enables rapid evaluation of layout-dependent mutual interactions, facilitating the optimization of array layouts. The method's accuracy is not inherently limited; error levels down to machine precision can be achieved, albeit at the cost of increased computational effort. Examples showed that EM simulations with irregular arrays comprising 256 wideband log-periodic antennas can be completed in just 10 min on a current laptop, with an additional minute to recompute the EEPs for a new layout. This corresponds to speed-up factors of 25 and 250, respectively, compared with FEKO's MLFMM running on a much larger workstation. The broadband SDM expansion could also be applied to the scattering analysis of rough surfaces or planar arrays of dissimilar antennas through its integration into an iterative solver.

Appendix
Harmonic Expansion of Complex Patterns

Let us start with the Fourier spectrum of basis function m

$$\tilde{\mathbf{f}}_m(\mathbf{k}) = \int\int_{S_m} \mathbf{f}_m(\mathbf{r})\; e^{-j\mathbf{k}\cdot(\mathbf{r}-\mathbf{r}_\mathbf{j})}\; \mathrm{d}S_m. \tag{28}$$

Then, substituting the Jacobi–Anger expansion of the plane-wave exponential [46] leads to

$$\tilde{\mathbf{f}}_m(k_z,\alpha) = \sum_{n=-\infty}^{\infty} \mathbf{a}_{mn}(k_z,\alpha)\; e^{jn\alpha} \tag{29}$$

with the vector coefficients given by

$$\mathbf{a}_{mn}(k_z,\alpha) = \int\int_{S_m} \mathbf{f}_m(\mathbf{r})\ J_n\big(k_\rho\rho\big)\ e^{-jn\phi}\ e^{-jk_z z}\ \mathrm{d}S_m \tag{30}$$

where J_n is the first-kind Bessel's function of order n. Given that the complex pattern reads $\mathbf{p}_m = \eta/(2j\lambda)(\tilde{\mathbf{f}}_m - (\tilde{\mathbf{f}}_m \cdot \mathbf{k})\ \mathbf{k}/k^2)$ and the TE and TM polarization vectors $\hat{\mathbf{e}}_{TE} = \hat{z}\times\mathbf{k}/k_\rho$ and $\hat{\mathbf{e}}_{TM} = \hat{\mathbf{e}}_{TE}\times\mathbf{k}/k$, we can derive the harmonic coefficients for TE–TM components of the complex pattern

$$p_{m,q}\big(k_z,\alpha\big) = \sum_{n=-\infty}^{\infty} c_{mn,q}\big(k_z,\alpha\big)\ e^{jn\alpha} \tag{31}$$

with $q = \{TE, TM\}$ and

$$\begin{aligned} c_{mn,TE} &= k_z/(2k)\big(a_{n+1,x} + a_{n-1,x} + ja_{n+1,y} \\ &\qquad - ja_{n-1,y}\big) - a_{n,z}k_\rho/k \\ c_{mn,TM} &= 1/2\big(- ja_{n+1,x} + ja_{n-1,x} + a_{n+1,y} \\ &\qquad + a_{n-1,y}\big). \end{aligned} \tag{32}$$

References

[1] G. Virone et al., "Strong mutual coupling effects on LOFAR: Modeling and in situ validation," *IEEE Trans. Antennas Propag.*, vol. 66, no. 5, pp. 2581–2588, May 2018.

[2] T. S. Bird, *Mutual Coupling Between Antennas*. Hoboken, NJ, USA: Wiley, 2021.

[3] D. B. Davidson, R. B. Wyath, and D. Ung, "Evaluation of alternative SKA-low station layouts," in *Proc. 35th Gen. Assem. Sci. Symp. Int. Union Radio Sci. (URSI GASS)*, Aug. 2023, pp. 1–4.

[4] N. Razavi-Ghods, E. de Lera Acedo, A. El-Makadema, P. Alexander, and A. Brown, "Analysis of sky contributions to system temperature for low frequency SKA aperture array geometries," *Exp. Astron.*, vol. 33, no. 1, pp. 141–155, Mar. 2012.

[5] J. Huang, "A technique for an array to generate circular polarization with linearly polarized elements," *IEEE Trans. Antennas Propag.*, vol. AP-34, no. 9, pp. 1113–1124, Sep. 1986.

[6] A. B. Smolders and H. J. Visser, "Low side-lobe circularly-polarized phased arrays using a random sequential rotation technique," *IEEE Trans. Antennas Propag.*, vol. 62, no. 12, pp. 6476–6481, Dec. 2014.

[7] T. D. Carozzi, P. Bolli, R. Subrahmanyan, and R. Braun, "Differentially rotated SKALA4.1 antennas in vogel configurations," in *Proc. 35th Gen. Assem. Sci. Symp. Int. Union Radio Sci. (URSI GASS)*, Aug. 2023, pp. 1–4.

[8] T. Latha, G. Ram, G. A. Kumar, and M. Chakravarthy, "Review on ultra-wideband phased array antennas," *IEEE Access*, vol. 9, pp. 129742–129755, 2021.

[9] R. Maaskant, R. Mittra, and A. Tijhuis, "Fast analysis of large antenna arrays using the characteristic basis function method and the adaptive cross approximation algorithm," *IEEE Trans. Antennas Propag.*, vol. 56, no. 11, pp. 3440–3451, Nov. 2008.

[10] E. de Lera Acedo, H. Pienaar, and N. Fagnoni, "Antenna design for the SKA1-LOW and HERA super radio telescopes," in *Proc. Int. Conf. Electromagn. Adv. Appl. (ICEAA)*, Cartagena des Indias, Colombia, Sep. 2018, pp. 636–639.

[11] B. R. Saliwanchik et al., "Mechanical and optical design of the HIRAX radio telescope," *Proc. SPIE*, vol. 11445, pp. 1047–1067, Jan. 2021.

[12] P. Bolli, M. Bercigli, P. Di Ninni, L. Mezzadrelli, and G. Virone, "Impact of mutual coupling between SKALA4.1 antennas to the spectral smoothness response," *J. Astronomical Telescopes, Instrum., Syst.*, vol. 8, no. 1, pp. 11–23, Feb. 2022.

[13] R. F. Harrington, *Field Computation By Moment Methods*. Piscataway, NJ, USA: IEEE Press, 1993.

[14] N. Engheta, W. D. Murphy, V. Rokhlin, and M. S. Vassiliou, "The fast multipole method (FMM) for electromagnetic scattering problems," *IEEE Trans. Antennas Propag.*, vol. 40, no. 6, pp. 634–641, Jun. 1992.

[15] D. B. Davidson et al., "Electromagnetic modelling of the SKA-LOW AAVS2 prototype," in *Proc. 33rd Gen. Assem. Sci. Symp. Int. Union Radio Sci.*, Rome, Italy, Sep. 2020, pp. 1–4.

[16] D. J. Ludick, R. Maaskant, D. B. Davidson, U. Jakobus, R. Mittra, and D. I. L. de Villiers, "Efficient analysis of large aperiodic antenna arrays using the domain Green's function method," *IEEE Trans. Antennas Propag.*, vol. 62, no. 4, pp. 1579–1588, Apr. 2014.

[17] H. Bui-Van et al., "Fast and accurate simulation technique for large irregular arrays," *IEEE Trans. Antennas Propag.*, vol. 66, no. 4, pp. 1805–1817, Apr. 2018.

[18] A. S. Conradie and M. M. Botha, "Preconditioned localized-solution iterative solver with nested cross approximation for large arrays," *IEEE Trans. Antennas Propag.*, vol. 72, no. 8, pp. 6584–6598, Aug. 2024.

[19] D. Gonzalez-Ovejero and C. Craeye, "Interpolatory macro basis functions analysis of non-periodic arrays," *IEEE Trans. Antennas Propag.*, vol. 59, no. 8, pp. 3117–3122, Aug. 2011.

[20] C. Craeye, "A fast impedance and pattern computation scheme for finite antenna arrays," *IEEE Trans. Antennas Propag.*, vol. 54, no. 10, pp. 3030–3034, Oct. 2006.

[21] L. Gurel and W. C. Chew, "Fast algorithm for scattering from planar arrays of conducting patches," *IEEE Microw. Guided Wave Lett.*, vol. 8, no. 4, pp. 155–157, Apr. 1998.

[22] E. Suter and J. R. Mosig, "A subdomain multilevel approach for the efficient MoM analysis of large planar antennas," *Microw. Opt. Technol. Lett.*, vol. 26, no. 4, pp. 270–277, Aug. 2000.

[23] V. V. S. Prakash and R. Mittra, "Characteristic basis function method: A new technique for efficient solution of method of moments matrix equations," *Microw. Opt. Technol. Lett.*, vol. 36, no. 2, pp. 95–100, Jan. 2003.

[24] L. Matekovits, V. A. Laza, and G. Vecchi, "Analysis of large complex structures with the synthetic-functions approach," *IEEE Trans. Antennas Propag.*, vol. 55, no. 9, pp. 2509–2521, Sep. 2007.

[25] Q. Gueuning, E. de Lera Acedo, A. K. Brown, and C. Craeye, "An inhomogeneous plane-wave based single-level fast direct solver for the scattering analysis of extremely large antenna arrays," *IEEE Trans. Antennas Propag.*, vol. 70, no. 10, pp. 9511–9523, Oct. 2022.

[26] V. Jandhyala, E. Michielssen, S. Balasubramaniam, and W. C. Chew, "A combined steepest descent-fast multipole algorithm for fast analysis of 3D scattering by rough surfaces," *IEEE Trans. Geosci. Remote Sens.*, vol. 36, no. 3, pp. 738–748, May 1998.

[27] A. Freni, P. De Vita, P. Pirinoli, L. Matekovits, and G. Vecchi, "Fast-factorization acceleration of MoM compressive domain-decomposition," *IEEE Trans. Antennas Propag.*, vol. 59, no. 12, pp. 4588–4599, Dec. 2011.

[28] J.-S. Zhao and W. C. Chew, "MLFMA for solving integral equations of 2-D electromagnetic problems from static to electrodynamic," *Microw. Opt. Technol. Lett.*, vol. 20, no. 5, pp. 306–311, Mar. 1999.

[29] K. Zhao, M. N. Vouvakis, and J.-F. Lee, "The adaptive cross approximation algorithm for accelerated method of moments computations of EMC problems," *IEEE Trans. Electromagn. Compat.*, vol. 47, no. 4, pp. 763–773, Nov. 2005.

[30] Q. Gueuning, E. de Lera Acedo, E. Colin-Beltran, and C. Craeye, "Mutual coupling analysis of large irregular arrays: From multipole to interpolatory methods," in *Proc. 9th Eur. Conf. Antennas Propag. (EuCAP)*, Lisbon, Portugal, Apr. 2015, pp. 1–4.

[31] L. J. Jiang and W. C. Chew, "A mixed-form fast multipole algorithm," *IEEE Trans. Antennas Propag.*, vol. 53, no. 12, pp. 4145–4156, Dec. 2005.

[32] H. Cheng et al., "A wideband fast multipole method for the Helmholtz equation in three dimensions," *J. Comput. Phys.*, vol. 216, no. 1, pp. 300–325, Jan. 2006.

[33] O. Ergul and B. Karaosmanoglu, "Broadband multilevel fast multipole algorithm based on an approximate diagonalization of the Green's function," *IEEE Trans. Antennas Propag.*, vol. 63, no. 7, pp. 3035–3041, Jul. 2015.

[34] T. Xia, L. L. Meng, Q. S. Liu, H. H. Gan, and W. C. Chew, "A low-frequency stable broadband multilevel fast multipole algorithm using plane wave multipole hybridization," *IEEE Trans. Antennas Propag.*, vol. 66, no. 11, pp. 6137–6145, Nov. 2018.

[35] I. Bogaert, J. Peeters, and F. Olyslager, "A non-directive plane-wave MLFMA stable at low frequencies," *IEEE Trans. Antennas Propag.*, vol. 56, no. 12, pp. 3742–3767, Dec. 2008.

[36] L. J. Jiang and W. C. Chew, "Low-frequency fast inhomogeneous plane-wave algorithm (LF-FIPWA)," *Microw. Opt. Technol. Lett.*, vol. 40, no. 2, pp. 117–122, Jan. 2004.

[37] H. Wallén and J. Sarvas, "Translation procedures for broadband MLFMA," *Prog. Electromagn. Res.*, vol. 55, pp. 47–78, 2005.

[38] D. Wulf and R. Bunger, "An efficient implementation of the combined wideband MLFMA/LF-FIPWA," *IEEE Trans. Antennas Propag.*, vol. 57, no. 2, pp. 467–474, Feb. 2009.
[39] W. C. Chew, J. M. Jin, E. Michielssen, and J. Song, *Fast and Efficient Algorithms in Computational Electromagnetics*. Norwood, MA, USA: Artech House, 2001.
[40] I. Bogaert, D. Pissoort, and F. Olyslager, "A normalized plane-wave method for 2D Helmholtz problems," *Microw. Opt. Technol. Lett.*, vol. 48, no. 2, pp. 237–243, Feb. 2006.
[41] L. L. Meng, M. Hidayetoglu, T. Xia, W. E. I. Sha, L. J. Jiang, and W. C. Chew, "A wideband 2-D fast multipole algorithm with a novel diagonalization form," *IEEE Trans. Antennas Propag.*, vol. 66, no. 12, pp. 7477–7482, Dec. 2018.
[42] W. C. Chew and C. C. Lu, "A fast algorithm to compute the wave-scattering solution of a large strip," *J. Comput. Phys.*, vol. 107, no. 2, pp. 378–387, Aug. 1993.
[43] FEKO. *Electromagnetic Simulation Software*. Accessed: Jan. 18, 2025. [Online]. Available: https://www.feko.info
[44] J. A. Kong, *Theory of Electromagnetic Waves*. Hoboken, NJ, USA: Wiley, 1975.
[45] Q. Gueuning, C. Craeye, and C. Oestges, "Sampling rules for an inhomogeneous plane-wave representation of scattered fields," *IEEE Trans. Antennas Propag.*, vol. 67, no. 3, pp. 1697–1708, Mar. 2019.
[46] M. Abramowitz and I. A. Stegun, *Handbook of Mathematical Functions With Formulas, Graphs, and Mathematical Tables*. New York, NY, USA: Dover, 1965.
[47] D. Gonzalez-Ovejero, F. Mesa, and C. Craeye, "Accelerated macro basis functions analysis of finite printed antenna arrays through 2D and 3D multipole expansions," *IEEE Trans. Antennas Propag.*, vol. 61, no. 2, pp. 707–717, Feb. 2013.
[48] A. J. Faulkner et al., "SKA Memo 122: The aperture arrays for the SKA: The SKADS white paper," Univ. Manchester, Manchester, U.K., Tech. Rep. 122, 2010. [Online]. Available: https://research.manchester.ac.uk/en/publications/memo-122-the-aperture-arrays-for-the-ska-the-skads-white-paper
[49] D. Anstey et al., "Mitigating zenith blindness from mutual coupling in a sunflower phased array," in *Proc. 18th Eur. Conf. Antennas Propag. (EuCAP)*, Glasgow, U.K., Mar. 2024, pp. 1–5.

Quentin Gueuning received the Ph.D. degree from the Université catholique de Leuven (UCLouvain), Leuven-la-Neuve, Belgium, in 2019.

He is currently a Senior Research Associate with the University of Cambridge, Cambridge, U.K., where he is a member of the Astrophysics Group and the Kavli Institute for Cosmology, Cavendish Laboratory. He also contributes to the Data Processing Agile Release Train of the SKAO, focusing on software development for the Square Kilometer Array Telescope. His research interests include fast computational methods, asymptotic high-frequency theories, mutual coupling analysis, array and antenna design and measurements, and calibration and forward modeling of radio telescopes.

Eloy de Lera Acedo received the Ph.D. degree from the University Carlos III of Madrid, Leganes, Spain, in 2010.

He is currently an Associate Professor with the Cavendish Laboratory, University of Cambridge, Cambridge, U.K., where he is the Head of the Radio Astronomy and Cosmology Research Group, Cavendish Astrophysics. In 2019, he Co-Founded Cambridge Electromagnetic Technology Ltd. (CEMTL), Cambridge. He leads development activities at Cambridge for the upcoming SKA radio telescope and sits on the Executive Board of the HERA experiment. He is the international PI of the REACH telescope and the CosmoCube space mission, both aiming at the detection and study of the redshifted 21-cm line from the infant universe (Dark Ages, Cosmic Dawn, and the Epoch of Re-Ionization). In the past, he led the antenna and low-noise amplifier work package of the SKA LFAA Aperture Array Design Consortium, which developed the array stations for the SKA1-LOW telescope. For the Hydrogen Epoch of Re-ionization Array (HERA), he led the design of the wideband feed within the analog team. His research interests include from ultrawideband array and antenna design, electromagnetic modeling, telescope calibration, and low-noise systems to the broader science case of 21-cm cosmology experiments.

Anthony Keith Brown (Life Senior Member, IEEE) has been working in the field of antennas since 1974. He is currently an Emeritus Professor of radiative electromagnetics with Queen Mary, University of London, London, U.K., and an Emeritus Professor of communications engineering with the University of Manchester, Manchester, U.K., where he was the Head of the School of Electrical and Electronic Engineering. Since 2016, he has been a Former Associate Dean for Teaching and Learning with the University of Manchester. He founded EASAT Antennas Ltd. (now Easat Radar Systems), Stoke-on-Trent, U.K., in 1987, where he has been a CTO, a CEO, and a Company Chairman. His research has resulted in more than 150 publications including five patents and, as co-authored, two books. His research interests include antennas and propagation. He now concentrates on the applications of broadband antennas to radar, communications, and radio astronomy and on the characterization of large electromagnetic structures.

Mr. Brown is a fellow of the Institution of Engineering Technology and the Institution of Mathematics and Its Applications.

Christophe Craeye (Senior Member, IEEE) was born in Belgium, in 1971. He received the master's degree in electrical engineering and the Ph.D. degree in applied sciences from the Université catholique de Leuven (UCLouvain), Leuven-la-Neuve, Belgium, in 1994 and 1998, respectively.

His Ph.D. was carried out in collaboration with the National Aeronautics and Space Administration (NASA), Washington, DC, USA, and the European Space Agency (ESA), Paris, France. From 1999 to 2001, he was a Post-Doctoral Researcher with Eindhoven University of Technology, Eindhoven, The Netherlands. Since 1999, he has been with the University of Massachusetts, Amherst, MA, USA. Since 2001, he has been with The Netherlands Institute for Research in Astronomy, Dwingeloo, The Netherlands. Since 2002, he has been started an antenna research activity with UCLouvain, Ottignies-Louvain-la-Neuve, Belgium, where he is currently a Professor. Since 2011, he has been with the Astrophysics and Detectors Group, University of Cambridge, Cambridge, U.K. His research is funded by the Région Wallonne, the European Commission, ESA, the Fonds National de la Recherche Scientifique (FNRS), and UCLouvain. His current research interests include mutual coupling, finite antenna arrays, wideband antennas, small antennas, metasurfaces, and numerical methods for fields in periodic media, with applications to communication and sensing systems.

Dr. Craeye received the 2005–2008 Georges Vanderlinden Prize from the Belgian Royal Academy of Sciences in 2009. He was an Associate Editor of IEEE TRANSACTIONS ON ANTENNAS AND PROPAGATION from 2004 to 2010 and IEEE ANTENNAS AND WIRELESS PROPAGATION LETTERS from 2011 to 2017.

Oscar O'Hara was born in Oxfordshire, U.K., in 1999. He received the B.A. degree in physics from Trinity College Dublin, Dublin, Ireland, in 2021. He is currently pursuing the Ph.D. degree with the Cavendish Laboratory, University of Cambridge, Cambridge, U.K.

From 2019 to 2021, he was a Part-Time Research Assistant with The Dublin Institute for Advanced Studies covering the very low-frequency monitoring of the Earth's ionosphere and the impacts of solar flares. His current research interests include development of a high-sensitivity Rydberg atomic sensor and the simulated analysis of potential systematics for the Square Kilometer Array.